Available online at www.sciencedirect.com
SCIENCE DIRECT®
Journal of Magnetic Resonance 159 (2002) 183–189
JMR Journal of Magnetic Resonance
www.academicpress.com

Euclidian distance-weighted smoothing for quantitative MRI: application to intervoxel anisotropy index mapping with DTI

Jean-Marie Bonny* and Jean-Pierre Renou

Structures Tissulaires et Interactions Moléculaires, INRA Theix, 63122 Saint-Genes-Champanelle, France

Received 28 May 2002; revised 16 August 2002

Abstract

During the computation of intervoxel anisotropy features, the inclusion of both eigenvalues and eigenvectors reduces the effect of noise, but spatial averaging blurs the resulting maps. We propose a new adaptive technique that uses data-dependent weights in the averaging process so that the influence of each neighbor in the local window is proportional to the similarity of characteristics of the neighbor considered to those of the reference central voxel. This likeness criterion is based on the multidimensional Euclidian distance using the entire available multispectral information contained in the diffusion-weighted images. This solution is controlled by a single parameter β that results from a compromise between edge-preserving and noise-smoothing abilities. This Euclidian distance-weighted technique is a generic solution for filtering noise during parametric reconstruction. It was applied to map anisotropy using an intervoxel lattice index (LI) from experimental images of mouse brain in vivo and achieves noise reduction without distorting small anatomical structures. We also show how to employ in the discrimination scheme the images not used in the estimation of the considered feature.

Keywords: MRI; Quantitative imaging; Multispectral filter; Diffusion

1. Introduction

Intervoxel anisotropy features were introduced by Pierpaoli and Basser [1] and extended by Skare et al. [2] to reduce the effect of noise, which makes the intravoxel anisotropy index dependent on the signal-to-noise ratio. The principle is to perform spatial averaging of indices based on both eigenvalues and eigenvectors.

It is now clear that including eigenvectors in the calculation improves the accuracy of the anisotropy indices [3,4] but the resulting maps are blurred by the spatial averaging. To circumvent the introduction of further partial volume effects, newer methods advocate averaging the anisotropy indices between acquisitions rather than in the spatial domain [2,5]. However, the local averaging process ought to be improved by excluding voxels with characteristics that are very different from those of the reference voxel, as suggested initially in [1]. We propose a new method that does not exclude voxels but weights the local averaging process by a multichannel Euclidian distance to reduce the influence, in the resulting index characterizing the diffusion anisotropy in the reference voxel, of those voxels that present very different characteristics. The likeness criterion is calculated from the set of N diffusion-weighted available images acquired in the different gradient directions defining the DTI protocol.

We evaluated the likeness criterion (i.e., the Euclidian distance) using diffusion data generated by Monte-Carlo simulations. The Euclidian distance weighting (EDW) process, which is controlled by a single parameter β, was tested by mapping the intervoxel lattice index (LI) from both simulated data sets and images of mouse brain obtained in vivo by microscopic MRI.

2. Background

The general form of a spatially averaged parameter p^* in the reference voxel with curvilinear coordinates $\mathbf{r}$ is

* Corresponding author. Fax: +33-4-73-62-45-21.
E-mail addresses: bonny@clermont.inra.fr (J.-M. Bonny), jpr@clermont.inra.fr (J.-P. Renou).

1090-7807/02/$ - see front matter © 2002 Elsevier Science (USA). All rights reserved.
PII: S1090-7807(02)00011-3

$$p^*(\mathbf{r}) = \frac{\sum_{i=1}^{K} w_i p(\mathbf{r}_i)}{\sum_{i=1}^{K} w_i}. \quad (1)$$

The curvilinear coordinates of voxels inside the local window of size K are denoted $\mathbf{r}_i$, $i = 1, 2, \ldots, K$. The likeness between the reference voxel in the window center and the ith voxel on the window is represented by the positive weight w_i. The greater the likelihood is of having two voxels with the same characteristics, the greater will be the weight w_i. The basic idea is to express the coefficients w_i as function of the data available in the local window. p^* is then the output of a data-dependent nonlinear filter applied on the p map, where p is any feature of interest calculated from the diffusion tensor images.

In this work, this concept of data-dependent spatial smoothing is applied for mapping the local intervoxel LI [1]. The basic element of the LI compares the anisotropic parts of the diffusion tensor in two voxels

$$\mathrm{LI}(\mathbf{r}) = \sqrt{\frac{3}{8}} \frac{\sqrt{\mathbf{d}(\mathbf{r}) : \mathbf{d}(\mathbf{r}_i)}}{\sqrt{\mathbf{D}(\mathbf{r}) : \mathbf{D}(\mathbf{r}_i)}} + \frac{3}{4} \frac{\mathbf{d}(\mathbf{r}) : \mathbf{d}(\mathbf{r}_i)}{\sqrt{\mathbf{D}(\mathbf{r}) : \mathbf{D}(\mathbf{r})}\sqrt{\mathbf{D}(\mathbf{r}_i) : \mathbf{D}(\mathbf{r}_i)}}, \quad (2)$$

where $\mathbf{d}$ represents the anisotropic part of the diffusion tensor $\mathbf{D}$, $\mathbf{r}_i$, and $\mathbf{r}$ the respective curvilinear coordinates of the neighbor and the reference voxel, and : the generalized tensor product. It was suggested initially to calculate the local intervoxel LI by spatially averaging each basic element over voxels that are contiguous to the reference voxel and weighting their contributions according to their distances [1]. We also used the data-dependent weighing function, which depends also locally on the likeness between the reference voxel and its neighbors.

Different acquisition schemes have been designed for DTI [6], each corresponding to the acquisition of a set of N ($N \geqslant 7$) diffusion-weighted images. A noisy magnitude vector $\mathbf{S} = [S_1 \quad S_2 \quad \ldots \quad S_N]^{\mathrm{T}}$ is then available in each voxel location. This vector-valued information should be used simultaneously to improve the immunity to noise of the likeness criterion. Euclidian distances have previously been used in the field of multichannel image filtering as a multichannel measure of unlikeness [7,8]. In our case, a scaled Euclidian distance was introduced

$$d_i = \sqrt{\frac{1}{N} \sum_{j=1}^{N} \frac{1}{2\sigma_j^2} [S_j(\mathbf{r}_i) - S_j(\mathbf{r})]^2}, \quad (3)$$

where σ_j^2 represents the variance of the jth component of the vector $\mathbf{S}$. When $S_j(\mathbf{r})$ and $S_j(\mathbf{r}_i)$ represent the same tissue types, the mean of $[S_j(\mathbf{r}_i) - S_j(\mathbf{r})]^2$ is $2\sigma_j^2$. By scaling the Euclidian distance by the two factors $2\sigma_j^2$ and N in Eq. (3), d_i is then dimensionless with a mean influenced by neither the signal-to-noise ratio nor the number N of diffusion-weighted images. An underlying assumption is that the noise is spatially stationary, indicating that σ_j^2 does not depend on voxel position $\mathbf{r}$ in each frame j, an assumption that has been verified in [9].

Finally, we have to define the relation between distance d_i and weight w_i. The two parameters are inversely related, because a large distance d_i, which expresses a high probability that the reference voxel $\mathbf{r}$ and its neighbor $\mathbf{r}_i$ have different characteristics, should correspond to a low weight w_i in the expression (1). For this purpose, we chose the following parametric transformation, which gives the value of w_i as function of d_i

$$w_i = a_i \exp(-\beta d_i), \quad \beta \geqslant 0. \quad (4)$$

With this exponential transformation, a single parameter β controls the non-linearity of the averaging process and w_i is normalized, being equal to unity in the ideal case of identical tissues without noise ($d_i = 0$).

The term a_i refers to the inverse of the distance between the reference voxel and its neighbor, i.e.

$$a_i = \|\mathbf{r}_i - \mathbf{r}\|^{-1}. \quad (5)$$

Contrary to the Euclidian distance d_i, the latter a_i is not signal-dependent. It takes into account the effect of non-isotropic sampling of the image space, which is due not only to the square lattice but also to the possible acquisition of non-isotropic voxels. Moreover it ensures that, when the EDW concept is applied to the mapping of intervoxel LI, the anisotropy index obtained is rotationally invariant.

3. Methods

3.1. Study of Euclidian distance discriminator

Monte-Carlo simulations were performed to assess the effect of noise on the scaled Euclidian distance. We considered a reference tissue with eigenvalues (principal diffusivities) of $\mathbf{D}$ comparable to those of muscle fiber tracts; $\lambda_1 = 1.0 \times 10^{-3}\,\mathrm{mm}^2/\mathrm{s}$, $\lambda_2 = \lambda_3 = 0.8 \times 10^{-3}\,\mathrm{mm}^2/\mathrm{s}$. This corresponds to a cylindrically symmetric diffusion ellipsoid for which the principal axes were assumed to coincide with those of the laboratory frame. Noise-free diffusion-weighted signal vector $\mathbf{S}^\dagger = [S_1^\dagger \; S_2^\dagger \ldots S_N^\dagger]^{\mathrm{T}}$ was generated using the $N = 12$ gradient direction DTI protocol proposed by Papadakis et al. [6]. The b-matrix is normalized to obtain an averaged diffusion attenuation of 1/3.

The Rician noise distribution affecting the noisy magnitude signal was simulated by adding two independent Gaussian noises on the true complex parts $S_i^\dagger \cos(\phi)$ and $S_i^\dagger \sin(\phi)$, where $S_i^\dagger$ is the true value and ϕ an arbitrary phase value set to 60°. Each noisy magnitude S_i ($i = 1, \ldots, N$) was generated by calculating the magnitude from the two complex parts. The Gaussian noise level was set to the same value for each component and the SNR of the data corresponding to zero diffusion

weighting was used to denote the SNR of the complete data set **S**.

To assess the effect of difference of tissue characteristics on Euclidian distance, the diffusion-weighted signal vector of a neighbor tissue was simulated (i) by changing the angle θ between the ellipsoid principal axis from 0 to 90 °, and (ii) by lowering the anisotropy of the neighbor tissue by changing the principal diffusivities from $\lambda_2 = \lambda_3 = 0.8 \times 10^{-3}\,\mathrm{mm^2/s}$ (initial anisotropy) to $\lambda_2 = \lambda_3 = 1.0 \times 10^{-3}\,\mathrm{mm^2/s}$ (isotropy), $\lambda_1 = 1.0 \times 10^{-3}\,\mathrm{mm^2/s}$ being unchanged. For each pair of tissues and a given SNR, the Euclidian distance was calculated using Eq. (3), and 10,000 replicates were performed.

3.2. Analysis of Euclidian distance weighting in intervoxel lattice index mapping from simulated images

Using the above approach, synthetic images of size $32 \times 64 \times 14$ (12 diffusion-weighted images and 2 references without diffusion weighting) were simulated to study the performance of the EDW process. They consisted of two contiguous homogeneous regions differing in their principal diffusivities, the left region being anisotropic and the right region isotropic ($\lambda_1 = \lambda_2 = \lambda_3 = 1.0 \times 10^{-3}\,\mathrm{mm^2/s}$). Two data sets were generated differing in the anisotropy of the left region: $\lambda_1 = 1.0 \times 10^{-3}\,\mathrm{mm^2/s}$ and $\lambda_2 = \lambda_3 = 0.8 \times 10^{-3}\,\mathrm{mm^2/s}$ (low anisotropy, LI = 0.075), $\lambda_1 = 1.0 \times 10^{-3}\,\mathrm{mm^2/s}$ and $\lambda_2 = \lambda_3 = 0.2 \times 10^{-3}\,\mathrm{mm^2/s}$ (high anisotropy, LI = 0.681).

According to Eq. (1) where $p = \mathrm{LI}$, EDW intervoxel LI maps were computed from the noisy diffusion-weighted images (for the calculation of the weights) and the diffusion tensor maps (for the calculation of the intervoxel LI).

3.3. Analysis of Euclidian distance weighting in intervoxel lattice index mapping from experimental DTI images acquired in vivo of mouse brain

The DTI experiment was performed on a C57BL/6J adult mouse anesthetized by inhalation of isoflurane. Experiments were performed on an Avance DRX400 micro-imaging system (Bruker, GmbH, Ettlingen, Germany) with a wide-bore (89-mm) vertical 9.4 T magnet. Diffusion-weighted images were recorded using a pulsed-gradient spin-echo sequence ($\delta = 2.5\,\mathrm{ms}$, $\Delta = 6.5\,\mathrm{ms}$). To minimize the total acquisition time ($T_{\mathrm{acq}} = 1\,\mathrm{h}\ 30\,\mathrm{min}$), the diffusion tensor was estimated from a low DW image and a series of six diffusion-weighted images with gradient pulses applied in non-collinear directions [10]. For all acquisitions, sagittal slices 1 mm thick were acquired with an in-plane resolution of $200 \times 200\,\mu\mathrm{m}^2$. Motion artifacts were reduced by non-synchronous averaging of 16 acquisitions [11]. As for synthetic images, EDW intervoxel LI maps were computed from the noisy diffusion-weighted images and the diffusion tensor maps. The SNRs were ≈75 for the low b-value image and ≈32 for the high b-value ($\approx 850\,\mathrm{s\,mm^{-2}}$) images.

4. Results

4.1. Study of Euclidian distance discriminator

The results of the numerical simulations are shown in Fig. 1, which gives the multichannel Euclidian distance

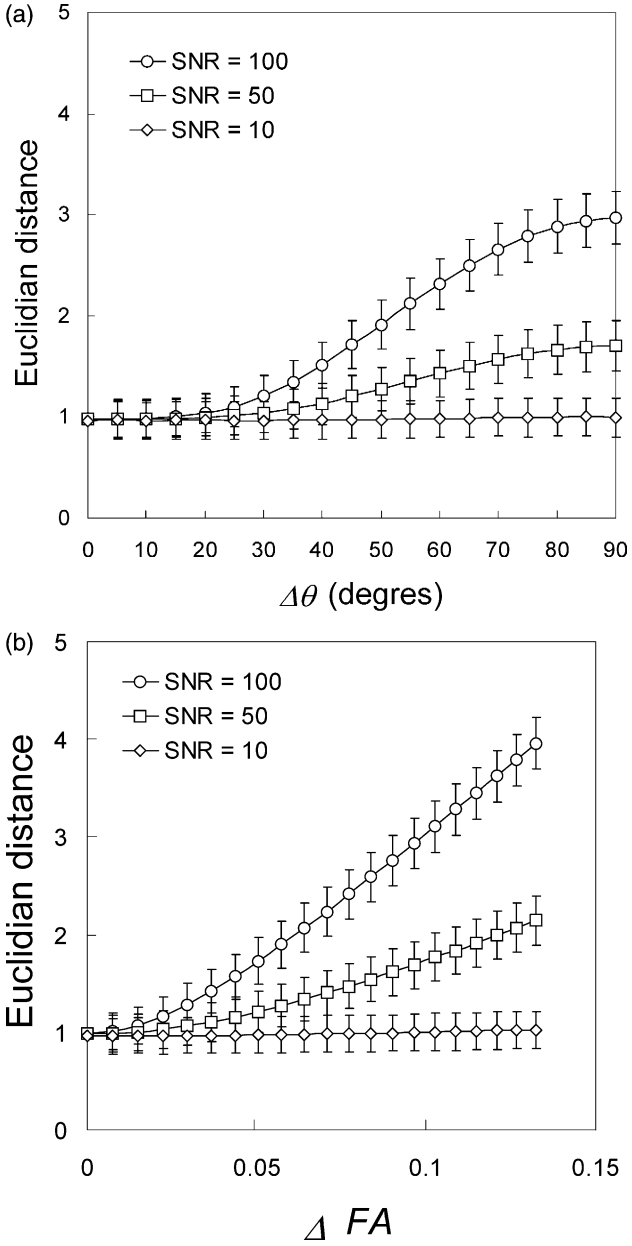

Fig. 1. Multichannel Euclidian distance as a function of the difference in diffusion characteristics between the neighbor voxel and the reference voxel. (A) The two voxels differ in the angle $\Delta\theta$ between the principal axes of their diffusion ellipsoids. (B) The two voxels differ in the difference ΔFA between their fractional anisotropies.

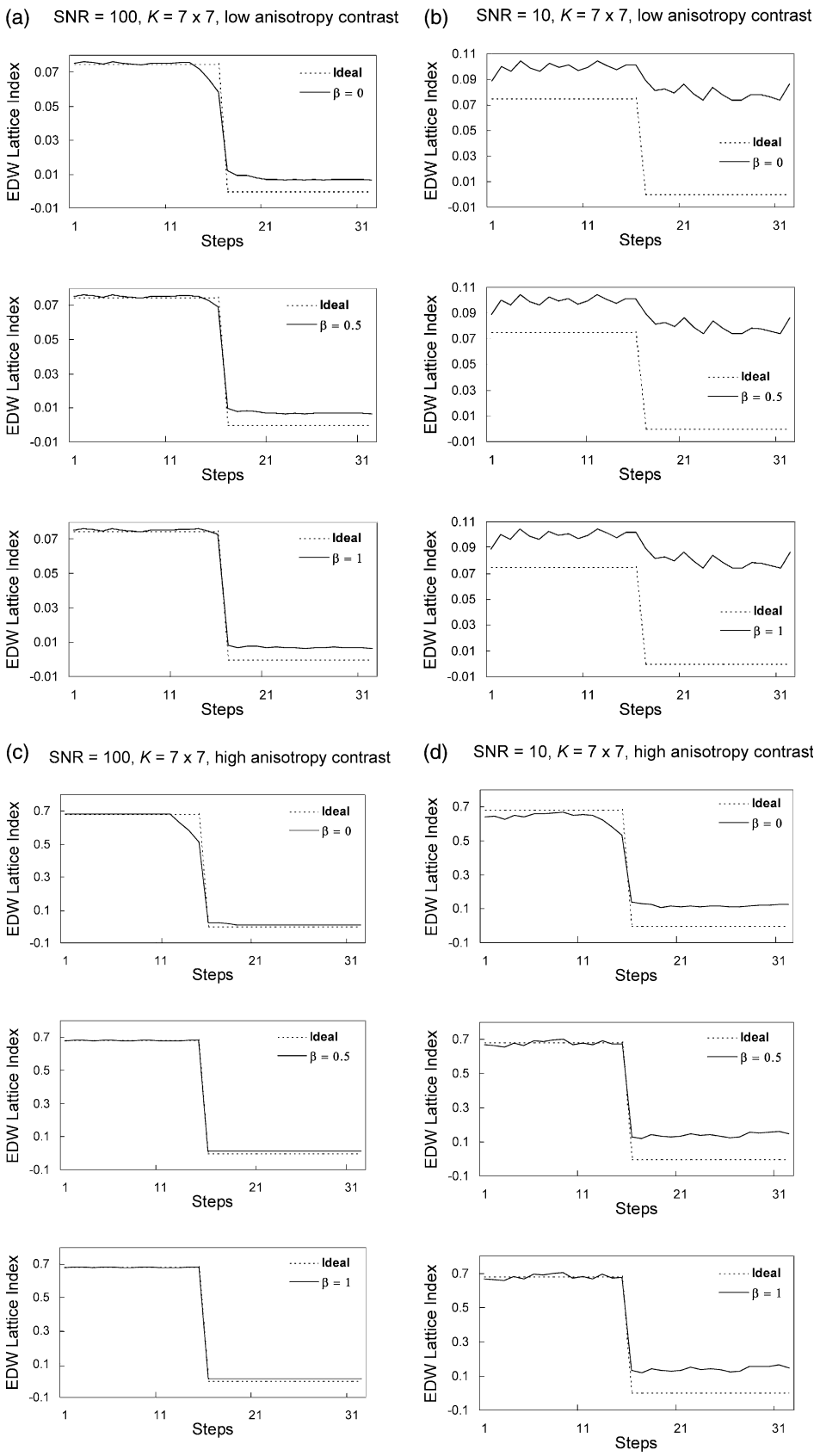

Fig. 2. Effect of β on the averaged horizontal profiles measured on the Euclidian distance weighted maps of the intervoxel LI for two different SNR values and two different anisotropy contrasts, $\beta = 0$ corresponds to intervoxel LI maps obtained as originally defined with constant spatial averaging, $\beta > 0$ resulting in locally data-dependent averaging.

defined by Eq. (3) as function of the difference in diffusion characteristics between the neighbor voxel and the reference voxel. In Fig. 1a, the two voxels differ in the angle $\Delta\theta$ between the principal axes of their diffusion ellipsoids from 0° to 90°. In Fig. 1b, the two voxels differ in their fractional anisotropy (FA) from 0 to 0.132. The latter value corresponds to the maximum difference when the reference voxel is characterized by $\lambda_1 = 1.0 \times 10^{-3}\,\mathrm{mm^2/s}$ and $\lambda_2 = \lambda_3 = 0.8 \times 10^{-3}\,\mathrm{mm^2/s}$ (FA = 0.132), whereas the neighbor voxel is isotropic $\lambda_1 = \lambda_2 = \lambda_3 = 1.0 \times 10^{-3}\,\mathrm{mm^2/s}$ (FA = 0).

In both cases, the Euclidian distance is evidently a true unlikeness criterion, because it increases with the difference between the diffusion characteristics of the two voxels. Also, the Euclidian distance increases with the SNR for a given value of $\Delta\theta$ or ΔFA. For example, an angle of 45° between the principal axis of the diffusion ellipsoids produces a mean Euclidian distance equal to 0.96 (SD = 0.19), 1.20 (SD = 0.22), and 1.71 (SD = 0.24) for respective SNR values of 10, 50, and 100. A moderate difference of fractional anisotropy $\Delta FA = 0.05$ produces approximately the same output levels with a mean Euclidian distance equal to 0.97 (SD = 0.18), 1.21 (SD = 0.22), and 1.73 (SD = 0.25) for respective SNR values of 10, 50, and 100.

4.2. Analysis of Euclidian distance weighting in intervoxel lattice index mapping

Fig. 2 shows the horizontal profiles averaged in the vertical direction (64 lines) obtained from the EDW intervoxel LI maps. The parameter β ranged from 0 (constant weighting) to 1 (non-linear data-dependent weighting) for two different SNR values, for two different anisotropy contrasts between the left and right regions and a constant neighborhood size $K = 7 \times 7$.

At a high SNR of 100 (see Figs. 2a and c), the partial volume effect is dramatically reduced when β increases. This is expressed by a transition that approaches the ideal edge as β increases. Data-independent weighting ($\beta = 0$) produces marked edge distortions, with both underestimation and overestimation of anisotropy on each side of the transition. At a low SNR of 10, the increase of β reduces the partial volume effect only when the anisotropy contrast between the two contiguous regions is high (see Fig. 2d). When the anisotropy contrast is too low (see Fig. 2b), the result is independent of the value of β with a small transition between the two regions.

In the homogeneous regions away from the edge, intervoxel LI is offset by noise. This overestimation of anisotropy depends on the SNR and is always greater in the isotropic region. In the latter, the offset is equal to +0.007 and +0.080 for the respective SNRs = 100 and 10, whereas the offset is negligible in the anisotropic region. At the lowest SNR, and in the case of the lowest intrinsic anisotropy contrast (see Fig. 2c), these offsets reduce the contrast so that differentiation of the two regions becomes difficult.

Fig. 3 shows the SNR of the EDW intervoxel LI map in the anisotropic left region (LI = 0.075) as a function of parameter β for different SNR values of the diffusion-weighted images. The SNR of the EDW intervoxel LI map is defined by

$$\mathrm{SNR}(\mathrm{LI}^*) = 20 \log \frac{\mathrm{LI}^*(\beta)}{\sigma_{\mathrm{LI}^*}(\beta)}, \tag{6}$$

where $\sigma_{\mathrm{LI}^*}(\beta)$ represents the standard deviation of the EDW intervoxel LI feature for a given value of β. It indicates that noise level increases when β increases. This noise contamination is moderate (−2 dB when β goes from 0 to 10) and depends loosely on the SNR of the input diffusion-weighted images.

Fig. 4 compares anisotropy maps obtained on the same adult mouse brain in the sagittal plane. The noise sensitivity of the FA map represented in Fig. 4b is expressed by a global grainy aspect and falsely high-FA values in gray matter, for example in the cingular cortex (CGC). The intervoxel LI map with constant spatial averaging ($\beta = 0$, $K = 5 \times 5$) of Fig. 4c reduces the influence of noise by regularizing the anisotropy map. However, blur is introduced, which tends to lower the contrast between regions presenting differences in anisotropy. An intervoxel LI map with Euclidian distance-weighted smoothing ($\beta = 1$, $K = 5 \times 5$) of Fig. 4d shows both a reduced influence of noise with regularization of anatomical regions (for example, the cortical gray matter and the olfactory bulb OB), and a high contrast

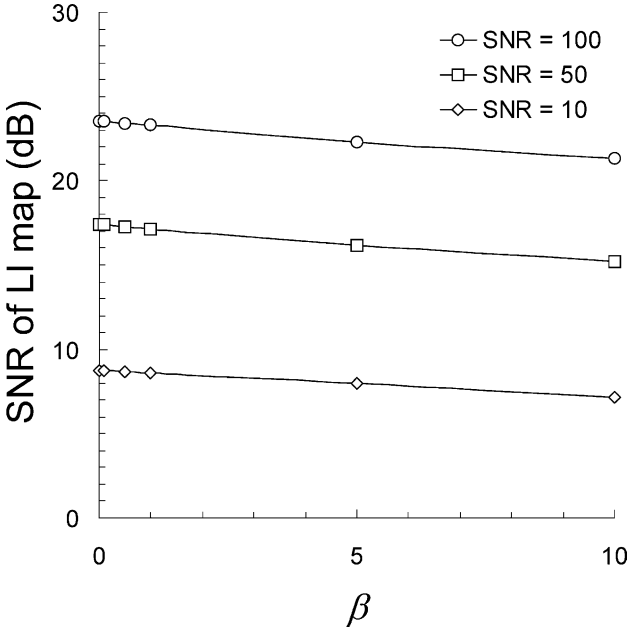

Fig. 3. Signal-to-noise ratio of the Euclidian distance-weighted maps of the intervoxel lattice index as a function of β.

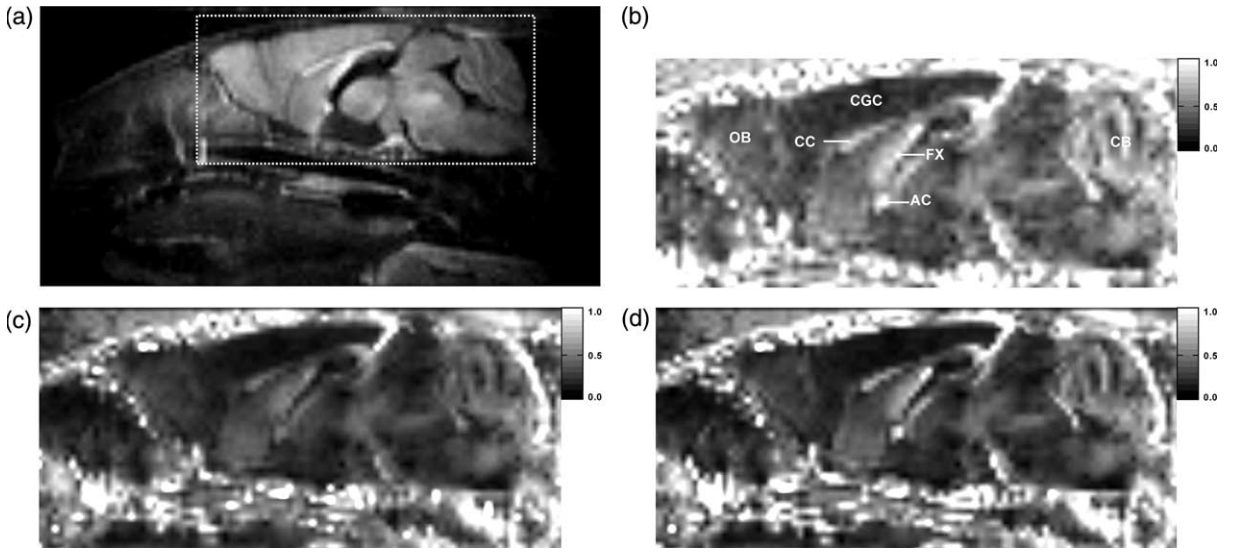

Fig. 4. Anisotropy maps of the same adult mouse brain obtained in vivo in the sagittal plane. (A) Diffusion-weighted image of the whole mouse head showing the region in which the following maps B–D are calculated. (b) Map of the fractional anisotropy (FA) index. (b) Map of the original intervoxel lattice index with constant spatial averaging ($\beta = 0$, $K = 5 \times 5$). (d) Map of the intervoxel lattice index with Euclidian distance-weighted smoothing ($\beta = 1$, $K = 5 \times 5$). OB, olfactory bulb; CC, *corpus callosum*; FX, fornix; AC, anterior commissure; CGC, cingular cortex; CB, *cerebellum.*

between regions presenting differences in anisotropy. The latter property reveals an increased anisotropy in several white matter tracts; in OB, *corpus callosum* (CC), fornix (FX), anterior commissure (AC) and *cerebellum* (CB). It should be noticed that the spatial resolution is sufficient to delineate effectively the microstructure of CB in both the diffusion-weighted image (see Fig. 4a) and the anisotropy maps (see Figs. 4b–d). The contrast between white matter and gray matter due to a difference in anisotropy leads to alternate bands that are corroborated by the photographs found in the histological atlas.

5. Discussion

The main advantage of feature mapping using EDW lies in its edge preserving property. It reduces the level of propagated noise while preventing introduction of a further partial volume effect. Basically, the edges (fine details) are better preserved as β increases, as demonstrated in both simulated and acquired images. Hence the choice of β results from a compromise between edge preservation and noise reduction, because β increase also induces a rise in propagated noise level in the resulting map (cf. Fig. 3). This is explained theoretically in the next section.

Fig. 1 shows that the discrimination between two voxels using Euclidian distance is highly dependent on the SNR. This gives a locally adaptive characteristic to EDW smoothing when β is not too low (which would impair its edge-preserving capability). When the SNR in the local window is low, it behaves in a linear fashion, favoring noise reduction. Conversely, when the SNR is high, any differences in tissue characteristics in the local window are detected with higher sensitivity (cf. Fig. 1), favoring edge preservation.

Owing to the edge preserving property, the size K of the local window has little influence on the shape of the transition when data-dependent weighting is chosen ($\beta > 0$). The size K of the local window mainly influences the level of noise reduction in the homogeneous regions. Assuming the different values of p in the local window result from independent measurements, the variance of the EDW parameter p^* is multiplied by the following noise reduction factor (NRF)

$$\mathrm{NRF} = \frac{\sum_{i=1}^{K} w_i^2}{\left(\sum_{i=1}^{K} w_i\right)^2}. \tag{7}$$

NRF is minimum for constant weights ($\beta = 0$) with $\mathrm{NRF} = K^{-1}$. For data-dependent weights ($\beta > 0$), NRF increases as depicted in Fig. 3.

EDW smoothing requires an estimate of the noise variance σ_j^2 (see Eq. (3)) in every image present. In practice, this is done by extracting magnitude values from a manually-placed region of interest in the image background [12]. Hence the estimate is not perfectly error-free, owing to the possible presence of ringing, motion and/or ghosting artifacts in the region of interest. Global under- (or over-) estimation of noise variance modifies the behavior of the EDW process which acts as increase (or an decrease) of β. If the estimation error is different for each frame, it induces an inappropriate scaling of the Euclidian distance of Eq. (3). Under- (or over-) estimation of noise variance σ_j^2 increases

(or decreases) erroneously the influence of the corresponding jth frame in d_i. Generally speaking, the method becomes more robust to these sporadic errors in the estimation of the noise variance as the number N of processed images increases in the EDW scheme.

To improve discrimination between regions, Euclidian distance weighting admits additional images (for example proton density- or T1-weighted), with the prerequisite that they are perfectly registered with the diffusion-weighted images. The Euclidian distance can easily integrate P additive images by spreading the sum of Eq. (3) from 1 to $N + P$. In this case, the variance σ_j^2 of each jth additive frame must be estimated [12] for appropriate scaling.

An alternative smoothing approach based on the application of the Perona–Malik non-linear filter to diffusion-weighted images prior to estimation of diffusion tensors has been proposed for the reduction of propagated noise in fractional anisotropy maps [13]. The main difference compared with our solution concerns the multispectral nature of EDW smoothing, which simultaneously uses the information contained in the diffusion-weighted images to define the frontiers between regions, whereas the Perona–Malik filter was applied separately. Considering the differences in both CNR and SNR between the different diffusion-weighted images, multispectral discrimination is preferable for defining the frontiers between regions with greater confidence and ensuring that the averaging process extends over the same areas. This justifies the development of multichannel techniques like the proposed EDW smoothing or a scheme specific to the regularization of diffusion tensor [14] which first restores the principal direction given by the tensor itself and then regularizes the tensor field in an anisotropic fashion using this restored direction. The EDW technique benefits from the possible application to any type of calculated parameter.

The proposed solution for quantitative MRI mapping belongs to the class of fuzzy adaptive filters for multispectral images. We discuss this solution for a given distance, the Euclidian one, and a given (fuzzy) transformation given by the exponential function of Eq. (4). The latter provides positive weights, ensuring the output of the weighted average is unbiased. The solution presented is efficient and simple, with a single parameter β controlling the non-linearity. Other schemes (distance/fuzzy transformations) have been proposed [15], but a comparison of the different solutions lies outside the scope of this paper [16].

We describe here an original solution for mapping intervoxel anisotropy features that circumvents the introduction of a further partial volume effect. We demonstrate its ability to produce anisotropy maps derived from low SNR diffusion-weighted images, such as those obtained in vivo by microscopic MRI. In addition, this EDW concept is a flexible solution for reducing the level of propagated noise in quantitative mapping because it can be easily extended to other features.

References

[1] C. Pierpaoli, P.J. Basser, Toward a quantitative assessment of diffusion anisotropy, Magn. Reson. Med 36 (1996) 893–906.

[2] S. Skare, T. Li, B. Nordell, M. Ingvar, Noise considerations in the determination of diffusion tensor anisotropy, Magn. Reson. Imaging 18 (2000) 659–669.

[3] K.M. Martin, N.G. Papadakis, C.L. Huang, L.D. Hall, T.A. Carpenter, The reduction of the sorting bias in the eigenvalues of the diffusion tensor, Magn. Reson. Imaging 17 (1999) 893–901.

[4] P.J. Basser, S. Pajevic, Statistical artifacts in diffusion tensor MRI (DT-MRI) caused by background noise, Magn. Reson. Med 44 (2000) 41–50.

[5] S.W. Sun, S.K. Song, C.Y. Hong, W.C. Chu, C. Chang, Improving relative anisotropy measurement using directional correlation of diffusion tensors, Magn. Reson. Med. 46 (2001) 1088–1092.

[6] N.G. Papadakis, D. Xing, C.L. Huang, L.D. Hall, T.A. Carpenter, A comparative study of acquisition schemes for diffusion tensor imaging using MRI, J. Magn. Reson. 137 (1999) 67–82.

[7] M. Pappas, I. Pitas, Multichannel distance filter, IEEE Trans. Signal Process. 47 (1999) 3412–3416.

[8] H. Soltanian-Zadeh, J.P. Windham, A.E. Yagle, A multidimensional non-linear edge-preserving filter for magnetic resonance image restoration, IEEE Trans. Image Process. 4 (1995) 147–161.

[9] E.R. McVeigh, R.M. Henkelman, M.J. Bronskill, Noise and filtration in magnetic resonance imaging, Med. Phys. 12 (1985) 586–591.

[10] P.J. Basser, C. Pierpaoli, A simplified method to measure the diffusion tensor from seven MR images, Magn. Reson. Med. 39 (1998) 928–934.

[11] N. Beckmann, B. Tigani, L. Mazzoni, J.R. Fozard, MRI of lung parenchyma in rats and mice using a gradient-echo sequence, NMR Biomed. 14 (2001) 297–306.

[12] J.M. Bonny, J.P. Renou, M. Zanca, Optimal measurement of magnitude and phase from MR data, J. Magn. Reson. 113 (1996) 136–144.

[13] G.J. Parker, J.A. Schnabel, M.R. Symms, D.J. Werring, G.J. Barker, Non-linear smoothing for reduction of systematic and random errors in diffusion tensor imaging, J. Magn. Reson. Imaging 11 (2000) 702–710.

[14] O. Coulon, D.C. Alexander, S.R. Arridge, A regularization scheme for diffusion tensor magnetic resonance images, Lecture Notes Comput. Sci. 2082 (2001) 92–105.

[15] I. Bloch, Information combination operators for data fusion: A comparative review with classification, IEEE Trans. Syst. Man Cybern. 26 (1996) 52–67.

[16] K.N. Plataniotis, D. Androutsos, A.N. Venetsanopoulos, Multichannel filters for image processing, Signal Process.: Image Commun. 9 (1997) 143–158.